ACS APPLIED MATERIALS & INTERFACES

Research Article

www.acsami.org

Enzyme Encapsulated Hollow Silica Nanospheres for Intracellular Biocatalysis

Feng-Peng Chang, Yann Hung, Jen-Hsuan Chang, Chen-Han Lin, and Chung-Yuan Mou*

Department of Chemistry, National Taiwan University, Taipei, Taiwan 10617

Supporting Information

ABSTRACT: Hollow silica nanospheres (HSN) with low densities, large interior spaces and permeable silica shells are suitable for loading enzymes in the cavity to carry out intracellular biocatalysis. The porous shell can protect the encapsulated enzymes against proteolysis and attenuate immunological response. We developed a microemulsion-templating method for confining horseradish peroxidase (HRP) in the cavity of HSN. This simple one-pot enzyme encapsulation method allows entrapping of the enzyme, which retains high catalytic activity. Compared with HRP supported on solid silica spheres, HRP@HSN with thin porous silica shells displayed better enzyme activity. The small HRP@HSN (~50 nm in diameter), giving satisfactory catalytic activity, can act as an intracellular catalyst for the oxidation of the prodrug indole-3-acetic acid to produce toxic free radicals for killing cancer cells. We envision this kind of hollow nanosystem could encapsulate multiple enzymes or other synergistic drugs and function as therapeutic nanoreactors.

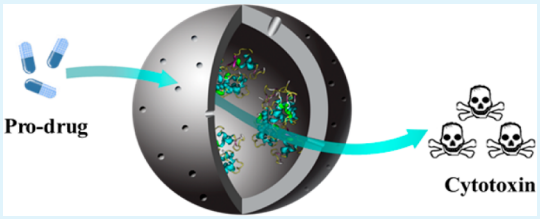

KEYWORDS: *hollow silica nanospheres, horseradish peroxidase, enzyme delivery, intracellular biocatalysis, nanoreactors*

1. INTRODUCTION

Cell organelles enclosed in membrane boundaries contain multiple enzymes to mediate signal transductions, negotiate metabolic reactions, and modify specific molecules to functional products. In a bio-inspired approach, encapsulating enzymes in hollow nanocarriers to create an optimal nanospace mimicking biocompartments will be very interesting. This nanoreactor would be suitable for biomedical applications such as enzyme replacement therapy or controlling cell fate.[1,2] The desirable nanoreactor should possess three functional domains: an interior reaction space, a permeable shell and the confined enzymes. In the cavity, enzymes are flexible and allow cascade reactions to occur. The outer shell should not only shield off external biological environments protecting interior enzymes from proteases digestion but also permit transport of generated active products to the cytoplasm. Furthermore, attenuate immunological responses may be expected.

To date, synthetic nanoreactors for intracellular delivery are still mostly at the conceptual stage. Reported examples are few and most are in test tube demonstrations. Only a few examples have been reported in cellular studies using protein−polymer systems.[3−9] Mesoporous silica has been shown to be a good material for encapsulating enzymes.[10−15] Enzyme immobilizations within various mesoporous materials such as MCM-41, SBA-15, FDU-12 and amorphous solid silica for biocatalysis have been comprehensively studied. However, most of the particles were large and few studies were applied in living cells.[16−18]

For biomedical delivery of this envisioned nanoreactor with size-selective permeating shell and large cavity, hollow-type mesoporous silica nanoparticles would be most desirable.[19−21] The encapsulate of agents of various functionalities, such as photoactive, magnetic or catalytic properties, inside the hollow cavity would further enhance its multifunctional applications. Recently, Huang et al. and Lim et al. synthesized hollow particles with large surface pores to trap proteins for delivery purposes.[22,23] Cao et al. reported hierarchically structured hollow silica that can be used to load enzymes via postsynthesis adsorption.[24] The enzyme loaded nanoparticles displayed good bioactivity, high enzyme stability and low leaching effect in a test tube study. However, it was not clear what the fraction of the loaded enzymes is inside the hollow particles. In addition, the micrometer size of the particles is not conducive to cellular uptake.

Current synthetic strategies to encapsulate enzymes in hollow nanostructures are tedious.[25] Hollow particles prepared from hard templating processes entail removal of the template by calcination or etching in a harsh condition. Either in situ encapsulation of enzymes during the preparation of hollow spheres or backfilling the interior cavity of hollow particles is challenging.[26] One then would either have destroyed the fragile enzymes if preloaded or have the difficult task of ship-in-bottle in enzyme loading after the shell was formed. In this work, we report a novel one-pot synthesis of horseradish peroxidase (HRP) encapsulated hollow silica nanspheres (HRP@HSN), based on templating reverse microemulsions. This water-in-oil (w/o) microemulsion approach employs an aqueous enzyme solution and allows entrapment of enzymes inside the final solid particles. Hollow silica nanoparticles with encapsulated enzymes were formed without any template-removing

Received: February 1, 2014
Accepted: April 2, 2014
Published: April 2, 2014

   dx.doi.org/10.1021/am500701c | ACS Appl. Mater. Interfaces 2014, 6, 6883−6890

processes after soaking in warm water with stirring (at 40 °C, 40 min). This approach is mild and the enzyme HRP could retain a high catalytic activity. Furthermore, the protected enzymes will be highly stable in a cellular environment. We will show the silica shell protects the enzymes against denaturants or proteolysis. Recently, Chiu et al. reported enzyme-encapsulated silica nanoparticles show some enzymatic function in "culture media".[27] However, a nanoreactor working in "living cells" to serve as an artificial biocompartment has not yet been achieved.

An active enzyme encapsulated hollow sphere with effectual catalytic activity, high stability, membrane permeability and cell biocompatibility offers a new direction for enzyme therapies. A challenging issue in cancer treatment is to reduce the side effects of the injected highly toxic anticancer agents. An enzyme therapy solution is to use enzymes that are able to convert a relatively nontoxic prodrug precursor into the active drug form. Although the prodrug is the inactive form and can be delivered to the blood, the products of the prodrug cleavage are highly cytotoxic and show their effect only in the vicinity of tumor cells. In this work, we test the encapsulated HRP in an enzyme−prodrug therapy strategy. With low cellular toxicity, the prodrug indole-3-acetic acid (IAA) had been suggested as a potential prodrug for cancer therapy because it could be transformed into free radicals by HRP.[28,29] The internal HRP in the porous hollow silica nanospheres will be shown to activate the prodrug indole-3-acetic acid (IAA) intracellularly to cytotoxic peroxyl radicals that trigger the killing of cancer cells. The concept of enzyme-prodrug is demonstrated on the particular HRP and IAA system based on hollow silica nanospheres.

2. EXPERIMENTAL SECTION

2.1. Synthesis of HRP@HSN, HRP supported on solid silica spheres (HRP@SSN), HSN and SSN. Solid/hollow silica nanospheres were synthesized by a reverse microemulsion method. Typically, 20 mL of decane, 1.63 mL of CA-520, 550 μL of *n*-hexanol and 350 μL of H_2O with or without HRP (1.3 mg/mL) were mixed at room temperature to generate the water-in-oil microemulsion. Then, silica sources (100 μL of tetraethylorthosilicate (TEOS) and 25 μL of ethanolic 3-aminopropyltrimethoxysilane (APTMS) solution) were added with stirring. The ethanolic APTMS solution was prepared by adding 200 μL of APTMS to 1.4 mL of absolute ethanol. After 10 min, 250 μL of aqueous ammonia (28−30 wt %) was introduced to the mixture and the mixture was stirred for 8 h at 20 °C. Then, 95% ethanol was added to destabilize the microemulsion system and solid products were centrifuged at 15,000 rpm for 15 min. To obtain the hollow structure, the samples were suspended in 70 mL of warm water (40 °C) and stirred for 40 min, isolated via centrifugation to obtain HRP@HSN or HSN (without adding HRP). HRP@SSN and SSN were prepared by the same procedure as above except eliminating APTMS and the water soaking step in the preparation.

2.2. Synthesis of HRP@F-HSN and F-HSN. F-HSN and HRP@F-HSN were synthesized by the aforementioned procedure, except that 25 μL of ethanolic FITC-APTMS solution was used in place of 25 μL of APTMS ethanolic solution. Ethanolic FITC-APTMS solution was prepared by adding 10 mg of fluorescein isothiocyanate and 200 μL of APTMS to 1.4 mL of absolute ethanol in the dark for 24 h under stirring.

2.3. HRP-Encapsulation Efficiency and Loading Yield. To determine encapsulation efficiency and loading yield, RITC-labeled HRP was prepared. HRP (3 mg) was dissolved in 0.1 M sodium bicarbonate solution (pH: 9) at a concentration of 6 mg/mL. Rhodamine B isothiocyanate (2.4 mg) was dissolved in 100 μL of dimethyl sulfoxide (DMSO) and 50 μL of dye solution was added to the protein solution. After the mixture was stirred for 12 h at 4 °C, the unreacted rhodamine B isothiocyanate was removed by dialysis and the HRP-RITC was encapsulated in HSN or SSN by the aforementioned method.

HRP-RITC@HSN (0.24 mg) or HRP-RITC@SSN (0.45 mg) was dissolved in 1 mL of NaOH (1N) and the amount of HRP-RITC encapsulated was read out from a calibration curve established by plotting the fluorescence of free HRP-RITC versus the concentration of HRP-RITC. HRP-encapsulation efficiency and loading yield were defined as the following: encapsulation efficiency (%) = mass of HRP-RITC in the HSN (SSN)/initial mass of HRP-RITC. Loading yield = mass of HRP-RITC in the HSN (SSN)/mass of HRP-RITC@HSN (HRP-RITC@SSN).

2.4. Characterization. The morphologic features and size of each product were characterized by TEM (Philips CM 100) at 80 kV, and images were recorded with a Gatan Orius CCD camera. Ethanolic suspension of sample was dropped onto a carbon-coated copper grid, air-dried and examined. For negative staining, the sample was soaked in 2% aqueous urayl acetate (UA) for 1 h with stirring. Then, a drop of the nanoparticle suspension was placed on a copper grid for imaging. Particle DLS size and zeta potential in deionized (DI) water, DMEM, and after stabilized with 2 mg/mL BSA in DMEM were measured by using a Zetasizer Nano (Malvern; Worcestershire, United Kingdom). Then, 0.35 mg of each sample with or without BSA stabilization was suspended in 1 mL test solutions. After ultrasonication for 3 min, solutions were transferred to 1 mL capillary cells for zeta assays, or transferred to plastic cuvettes for DLS measurements.

2.5. HRP Activity Assay. For the catalytic activity measurements, samples were suspended in 750 μL of sodium phosphate buffer solution (10 mM phosphate and 150 mM NaCl, pH 7.2) containing 80 μM H_2O_2. Then, 750 μL of *o*-phenylenediamine (o-PD) solution prepared in sodium phosphate buffer (0.4−3 mM) was added. After incubation for 1 h at room temperature, the absorption spectra of the oxidation products were recorded by a UV−vis spectrophotometer (Jasco, V-650). The kinetic study of the catalytic reaction was monitored using a microplate reader (Bio-Rad, model 680) at 415 nm (16 700 M^{-1} cm^{-1}) and Michaelis−Menten parameters (K_m, V_{max} and k_{cat}) were obtained using a Lineweaver−Burk plot ($1/v$ vs $1/[S]$, v = rate, S = concentration of the o-PD) and calculated from the fitting:

$$\frac{1}{\nu} = \frac{K_m}{V_{max}}\frac{1}{[S]} + \frac{1}{V_{max}}k_{cat} = \frac{V_{max}}{[E]}$$

2.6. Stability of Encapsulated HRP in the Presence of Trypsin and Urea. Because the high concentration of trypsin will intervene o-PD assay, we chose 3,3′,5,5′-tetramethylbenzidine (TMB) instead of o-PD to determine enzyme activity. Briefly, native HRP (1.6×10^{-3} μg) or HRP@HSN (3×10^{-2} μg) was incubated in 50 μL of phosphate citrate buffer containing 2 mg/mL trypsin at 50 °C. A phosphate citrate buffer (pH: 5.4) was prepared by 0.2 M Na_2HPO_4 and 0.1 M citric acid at a mixing ratio of 1.25:1 (v/v). After incubation for 1, 2 or 3 h, 850 μL of phosphate citrate buffer, 50 μL of TMB solution (0.02 M in DMSO) and 50 μL of H_2O_2 (0.02 M in DI water) were added. After 15 min, the absorption of TMB charge-transfer complex at 655 nm was determined.

To test the stability of protein against urea, native HRP (1.6×10^{-3} μg) or HRP@HSN (3×10^{-2} μg) was dispersed in 50 μL of phosphate citrate solution containing 6 M urea at 37 °C for 10, 30 or 60 min. Then, 850 μL of phosphate citrate buffer, 50 μL of TMB solution (0.02 M in DMSO) and 50 μL of H_2O_2 (0.02 M in DI water) were added. After 15 min, the absorption at 655 nm was determined.

2.7. Cell Culture. HeLa cells obtained from the American Type Culture Collection (Manassas, VA) were maintained in Dulbecco's modified eagles medium (DMEM; GIBCO) with 10% fetal bovine serum (FBS; GIBCO), 100 U/mL penicillin and 100 μg/mL streptomycin (GIBCO) at 37 °C in a humidified 5% CO_2 atmosphere. When adherent cells reached ∼60−70% confluence, they were detached with 0.25% trypsin-EDTA growth medium to allow for continued passaging.

2.8. Flow Cytometry Analysis. The uptake efficiency of particles by HeLa cells was determined by a FACSCalibur flow cytometer and

Scheme 1. Schematic Illustration for the Synthesis of Horseradish Peroxidase Encapsulated Hollow Silica Nanosphere (HRP@HSN)[a]

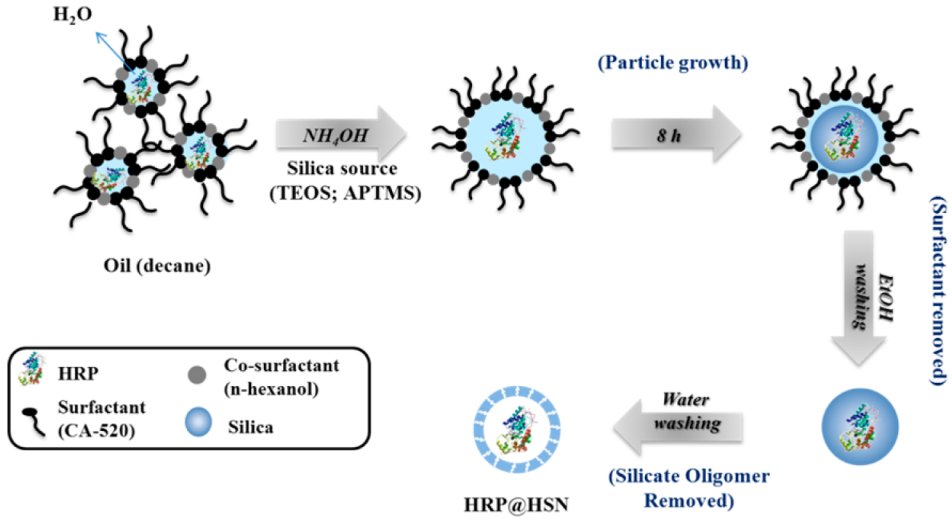

[a]HRP@HSN was obtained by the reverse water-in-oil (w/o) microemulsion system. TEOS: tetraethylorthosilicate. APTMS: 3-amino-propyltrimethoxysilane.

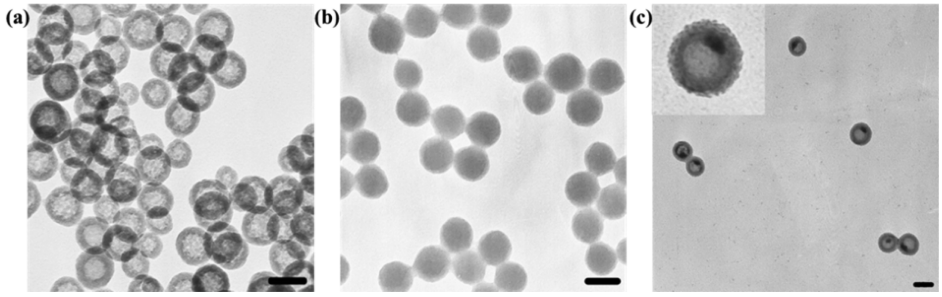

Figure 1. Transmission electron microscopy (TEM) images of horseradish peroxidase encapsulated silica nanospheres. (a) HRP@HSN, (b) HRP@SSN and (c) HRP@HSN stained with uranyl acetate (UA). UA-staining showed the enhanced electron density in the cavity of HSN. Scale bars are 50 nm.

CellQuest Pro software (Becton Dickenson, Mississauga, CA). The green emitting fluorescein dye incorporated in F-HSN and HRP@F-HSN serves as a marker to quantitatively determine their cellular uptake. Here, 2×10^5 cells were seeded in 6-well plates and allowed to attach for 24 h. Cells were incubated with 30, 60 or 100 μg/mL of BSA-stabilized particles in a serum-free medium for 2.5 h. Treated cells were then washed twice with PBS and then harvested by trypsinization. After centrifugation, the cells were resuspended in trypan blue solution to quench the fluorescence of particles adsorbed on the cell surface and flow cytometry analysis was carried out.

2.9. Confocal Fluorescence Microscopy Examination. Cells were seeded at the density of 2×10^5 cells per well in 6-well plates with cover glasses at the bottom of the wells and allowed to attach for 24 h. After incubation with BSA stabilized HRP@F-HSN or HRP-RITC@F-HSN (20 μg/mL) in serum-free medium for 2.5 h, cells were washed twice with PBS and then fixed in a 4% formaldehyde PBS solution at room temperature for 10 min. For actin skeleton staining, the cells were washed with PBS three times and incubated with 0.2% Triton X-100 and then 5% bovine serum albumin in PBS for 10 and 60 min, respectively. Rhodamine phalloidin was used for staining the filamentous actin skeleton at room temperature for 60 min. Then, treated cells were stained with 4′,6-diamidino-2-phenylindole (DAPI) in PBS (1 μg/mL) for 10 min at room temperature, washed twice with PBS, and then fluorescence images were obtained with a confocal microscope (TCS SP5, Leica).

2.10. Co-Localization Examination. Cells were seeded at the density of 2×10^5 cells per well in 6-well plates with cover glasses at the bottom of the wells and allowed to attach for 24 h. Cells were cocultured with an endosome marker *N*-(3-triethylammoniumpropyl)-4-(4-diethylaminophenylhexatrienyl)pyridinium dibromide (FM 4-64) (5 μg/mL) and BSA stabilized HRP@F-HSN (20 μg/mL) in serum-free medium. After 2.5 h of incubation, cells were washed twice with PBS and then fixed in a 4% formaldehyde PBS solution at room temperature for 10 min. Then, treated cells were stained with DAPI in PBS (1 μg/mL) for 10 min at room temperature, washed twice with PBS and then fluorescence images were obtained with a confocal microscope (TCS SP5, Leica).

2.11. Application of HRP@HSN for Cancer Therapy. A total of 2×10^4 cells were seeded in 24-well plates and allowed to attach for 24 h. To determine the dose effect of IAA on particle-treated cells, HeLa cells were incubated with BSA-stabilized HSN or HRP@HSN (100 μg/mL) for 2.5 h. After two washes with PBS, cells were exposed to IAA at different concentrations for 24 h. The cell viability was determined by WST-1 assay.

To determine the dose effect of native HRP and particles on cell viability, HeLa cells were incubated with BSA-stabilized HSN or HRP@HSN at concentrations of 60 and 100 μg/mL for 2.5 h. The doses of native HRP were equivalent to that of HRP encapsulated in 60 and 100 mg/mL HRP@HSN, respectively. After two washes with PBS, cells were exposed to 7.5 mM IAA for 24 h and cell viability was determined by a WST-1 assay.

Table 1. HRP Loading and Catalytic Activity of HRP@HSN, HRP@SSN and Native HPR

sample	HRP-encapsulation efficiency (%)[a]	loading yield (μg HRP/mg particle)[b]	K_m (μM)[c]	V_{max} (nM/s)[d]	turnover number[e] (k_{cat}) (s^{-1})	relative activity (%)
HRP@HSN	15.0 (±0.8)	18.6 (±2.3)	54.8 (±1.9)	2.65 (±0.1)	33.1 (±1.6)	47.1 (±2.3)
HRP@SSN	7.5 (±0.3)	5.4 (±0.2)	61.5 (±7.8)	2.47 (±0.1)	22.7 (±0.5)	32.4 (±0.7)
native HRP			43.0 (±7.9)	3.18 (±0.1)	70.0 (±1.9)	100 (±2.7)

[a]Encapsulated efficiency (%) = mass of HRP-RITC in the HSN (SSN)/initial mass of HRP-RITC. [b]Loading yield = mass of HRP-RITC in the HSN (SSN)/mass of the HRP-RITC loaded HSN(SSN). [c]K_m: A parameter related to the rate constant. [d]V_{max}: The maximum reaction velocity. [e]k_{cat}: Turnover number. K_m, V_{max} and k_{cat} were obtained using a Lineweaver–Burk plot. The k_{cat} value of native HRP was used as 100% catalytic activity.

3. RESULTS AND DISCUSSION

3.1. Synthesis and Characterization of Enzyme Encapsulated Nanospheres. HRP@HSN was synthesized by a modification of a water-in-oil (w/o) microemulsion templating approach reported in our earlier study.[30] In brief, an aqueous solution containing HRP was emulsified in an oil system containing a surfactant (isooctylphenyl ether, CA-520), cosurfactant (*n*-hexanol) and organic solvent (decane). After the silica sources tetraethoxysilane (TEOS) and amino-propyltrimethoxysilane (APTMS) and aqueous ammonia were introduced, the water-in-oil (w/o) mixture was stirred for 8 h at 20 °C to form HRP-entrapped silica nanoparticles. Hollow HRP@HSN was formed after the nanoparticles were further suspended in warm DI water (40 °C) for 40 min (Scheme 1) and washed with water, which is critical to the transformation of silica spheres to HSN.[30] We also synthesized HRP entrapped solid silica spheres, HRP@SSN, for activity comparison by eliminating APTMS and the water soaking step in the preparation. Transmission electron microscopy (TEM) images showed the enzyme encapsulated particles with a diameter of ∼50 nm (Figures 1a,b and S1, Supporting Information) and an internal hollow cavity of HRP@HSN with a diameter of about 30 nm. To confirm that HRP was entrapped in particles, HRP@HSN and HSN were negatively stained with uranyl acetate (UA). As shown in Figures 1c and S2 (Supporting Information) (in comparing with HSN without HRP (control)), the TEM images displayed an enhanced electron density inside HSN but no staining outside HSN was observed. This indicates that the enzyme was indeed mostly entrapped inside the hollow spheres. Dynamic light scattering (DLS) measurements (Table S1, Supporting Information) showed that the hydrodynamic sizes of HRP@HSN and HSN were 174.9 (±5.8) and 191.5 (±3.6) nm, respectively, indicating little aggregation of the nanoparticles. In addition, the nanoparticles showed positive zeta potentials in water, 20.5 (±0.5) and 21.6 (±0.5) mV, respectively (Table S1, Supporting Information). We carried out washing experiments to contrast the enzyme entrapment effect and adsorption effect between HSN and SSN (solid silica nanoparticle). We synthesized HRP-RITC (rhodamine B isothiocyanate labeled HRP) encapsulated in two kinds of nanoparticles, HSN and SSN, and employed them in the washing experiments (see the Supporting Information for the detailed method). In addition to the encapsulated in particles, the same amount of HRP-RITC (18.6 μg) (1 mg of HRP-RITC@HSN or 3.4 mg of HRP-RITC@SSN) was adsorbed onto the external surface of HSN or SSN by soaking with the nanoparticles for 60 min and these nanoparticles are served as control groups. All four kinds of nanoparticles were suspended in acidic DI water (pH 2.0) separately. At each washing cycle, the fluorescence of the nanoparticles was examined. After five washing cycles, almost no leakage of HRP-RITC from HRP-RITC@HSN or HRP-RITC@SSN was detected, whereas the adsorbed nanoparticles (controls) showed gradual-release of the HRP-RITC (Figure S3, Supporting Information). Therefore, washing experiments show that in HRP-RITC@HSN HRP was indeed encapsulated inside the hollow interior and entrapped in HSN.

Because the dye-doped nanoparticles displayed enhanced brightness in fluorescence,[31,32] which was attributed to the shielding effect, the encapsulation amount could not be determined directly from the fluorescence of the suspended nanoparticles. We determined the entrapped HRP-RITC in HRP-RITC@HSN and HRP-RITC@SSN by dissolving the nanoparticles in 1N NaOH and the amount of HRP-RITC encapsulated was determined from a calibration curve established by plotting the fluorescence of free HRP-RITC versus the concentration of HRP-RITC under the same condition (in 1N NaOH) (Figure S4, see the Supporting Information for the detailed method). The HRP encapsulation efficiency and loading yield are calculated and summarized in Table 1; approximately 15.0% and 7.5% of added HRP were encapsulated in HSN and SSN respectively, whereas each type of nanoparticles contained about 18.6 and 5.4 μg of HRP per milligram of HSN and SSN, respectively. The higher percentage of encapsulation of HRP in HSN is expected because the interior space is higher than the external surface. We note here that the efficiency of 15% is also higher than those reported for other nanoparticle systems generally.[33] This is probably due to the fact that enzymes are limited in the tiny water phase in the reverse w/o microemulsion. However, in this work, the amount of loading was deliberately kept low, so that protein aggregation within hollow spheres is avoided.

3.2. Activity of Encapsulated HRP. We examined the enzyme activity of HRP@HSN and HRP@SSN using *o*-phenylenediamine (o-PD) as the substrate.[34] Figure S5a (Supporting Information) is a dose-dependent UV–vis spectrum of o-PD showing successive oxidation of o-PD in the presence of HRP@HSN. The Lineweaver–Burk plot and Michaelis–Menten parameters (V_{max}, K_m and k_{cat}) of those entrapped enzymes along with native HRP are displayed in Figure S5b (Supporting Information) and Table 1. HRP@SSN (K_m = 61.5 μM) showed a higher K_m value than that of HRP@HSN (K_m = 54.8 μM) and native HRP (K_m = 43.0 μM). This indicated that different silica matrices may slightly affect the affinity between HRP and its substrate, o-PD. The turnover number of the HRP@HSN (k_{cat}: 33.1 s^{-1}) was less than that of native HRP (k_{cat}: 70.0 s^{-1}) but higher than that of HRP@SSN (k_{cat}: 22.7 s^{-1}). The enzyme activity of HRP@HSN and HRP@SSN was 47.1% and 32.4% of the native HRP, respectively. This decrease of catalytic activity for encapsulated enzymes is in agreement with literature reports on other systems[35] that may be attributed to the lowered diffusion rate of the substrates across silica shell to HRP. When HRP was entrapped in the silica spheres such as SSN, silica matrix hindering the access of

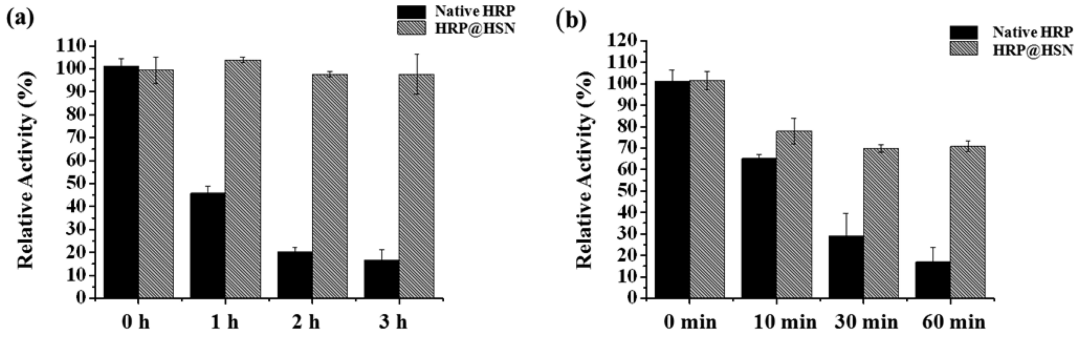

Figure 2. Stability of native HRP and HRP@HSN against denaturing environments. The enzymatic activity was measured after native HRP or HRP@HSN was treated with (a) 2 mg/mL trypsin at 50 °C or (b) 6 M urea at 37 °C at the indicated times. The relative activity of HRP was normalized to each sample before exposure to denaturing conditions.

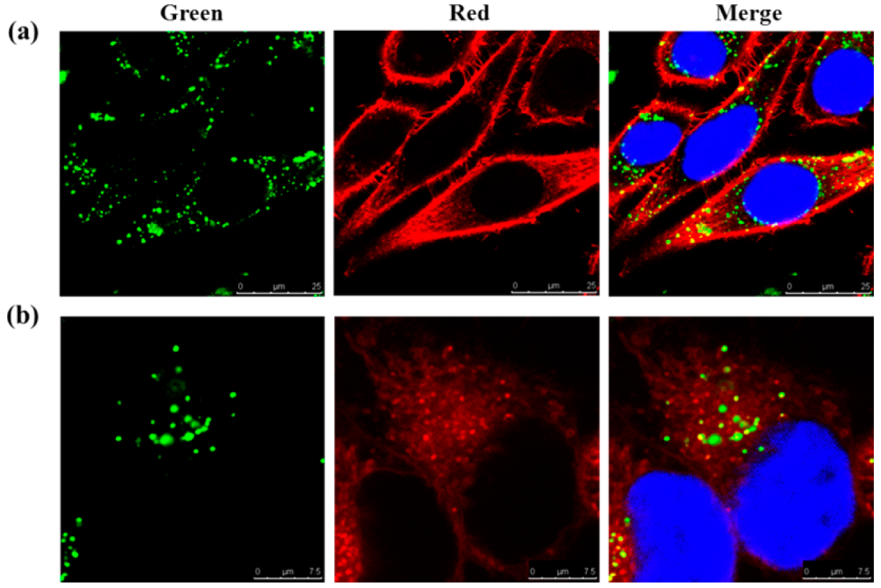

Figure 3. Confocal microscopy analysis of HRP@F-HSN in HeLa cells. (a) Internalization of HRP@F-HSN (green) by HeLa cells. The cell skeleton was stained with rhodamine phalloidin (red). (b) The cells treated with HRP@F-HSN were stained with the endosome-specific marker FM 4-64 (red, 5 μg/mL) and analyzed for an endosomal colocalization. The blue color is 4′,6-diamidino-2-phenylindole (DAPI)-stained nuclei.

the substrates and HRP@SSN showed the lowest catalytic activity. Thereafter, hollow spheres are examined further as a nanocarrier for enzyme activity.

3.3. Silica Shell Protects HRP. Poor stability and protease digestion are concerns in the enzyme-based therapeutics. We then examined the stability of HRP@HSN in the presence of a protease. As shown in Figure 2a, after exposure to 2 mg/mL trypsin at 50 °C for 3 h, native HRP lost almost all its activity, whereas activity of HRP@HSN still remained almost full, at about 98%. In comparison, in a recent report of HRP encapsulated in semipermeable polymer, only 20% activity remains after proteolysis.[33] Trypsin may be too big a molecule to diffuse across the silica shell. Next, we examined enzyme stability in the presence of the denaturant, urea. Figure 2b shows that after incubation with 6 M urea for 60 min, HRP@HSN maintained its activity at 71% of its initial activity whereas that of the native HRP only remained at 17%. Apparently, the barrier of the porous shell can prevent some of the urea diffusing into the interior of HSN. A few broken silica shells seem to have occurred in the urea environment in the initial 10 min of exposure but intact particles still kept enzyme stability stable afterward, so that the activity of HRP@HSN remained constant under 30−60 min of treatment. The significantly increased stability in the urea environment may also be partly due to the confinement effect of the hollow cavity where the 3D structure of the entrapped enzyme was difficult to unfold.

3.4. Cell Uptake of HRP@HSN. Up to now, hollow nanostructured materials have been used for diagnosis, cell imaging and stimuli-responsive drug release.[30,36,37] However, little has been reported on HSN to encapsulate enzymes for biomedical purposes. Also, we have shown the silica shell of HSN protected the interior HRP and possessed semipermeable properties of small molecules. These advantages provided opportunities for their uses in intracellular biocatalysis. For cellular studies, we then further characterized the physicochemical properties of nanoparticles in biological media. HRP@HSN exhibited a negative surface charge in the culture medium, DMEM, and significant aggregation of HRP@HSN occurred upon dispersal in DMEM (Table S1, Supporting Information). To improve the particle dispersion in a biological environment, we treated HRP@HSN with 2 mg/mL BSA.[38] DLS size indicated that BSA significantly improved particle dispersal in DMEM, probably due to the formation of protein corona on the particle surface.[39] The zeta values of BSA-coated HRP@HSN and HSN were −12 and −12.9 mV in DMEM, respectively.

dx.doi.org/10.1021/am500701c | ACS Appl. Mater. Interfaces 2014, 6, 6883−6890

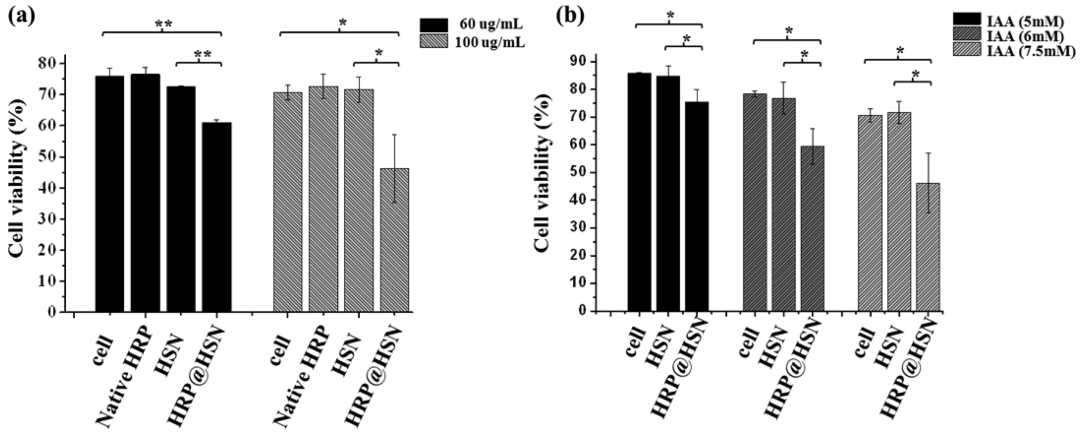

Figure 4. Cell viability of HRP@HSN- and HSN-treated cells in the presence of indole-3-acetic acid (IAA). (a) Dose effect of HRP@HSN, HSN and native HRP on cell viability. HeLa cells were treated with HRP@HSN or HSN at doses of 60 and 100 μg/mL for 2.5 h. The dose of native HRP was equivalent to that of HRP encapsulated in 60 and 100 mg/mL HRP@HSN. The cells were then washed with PBS and exposed to 7.5 mM IAA for 24 h. (b) Dose effect of IAA on particle-treated cells. HeLa cells were treated with or without 100 μg/mL particle for 2.5 h, followed by PBS washing and incubation with IAA at doses of 5, 6 and 7.5 mM for 24 h. The cell viability was processed with a WST-1 assay using 2-(4-iodophenyl)-3-(4-nitrophenyl)-5-(2,4-disulfophenyl)-2H-tetrazolium and normalized to cells only without any treatment. * p-value <0.05; ** p-value <0.001.

To visualize the cellular uptake of BSA-stabilized nanoparticles, we conjugated HRP@HSN and HRP-RITC@HSN with fluorescein isothiocyanate (FITC) to form HRP@F-HSN and HRP-RITC@F-HSN (see section 2 for the detailed method). Confocal microscopy images (Figure 3a) show that HRP@F-HSN (green channel) was internalized into cells. A colocalized image (Figure S6, Supporting Information, yellow channel) of F-HSN (green) and HRP-RITC (red) indicates HSN kept the enzymes steady in its interior cavity in the cellular environment for 24 h. We next employed flow cytometry to quantify the cell uptake of the nanoparticles. Figure S7 (Supporting Information) shows the remarkably high cellular uptake of HRP@F-HSN and F-HSN at the treated doses of 30, 60 and 100 μg/mL for 2.5 h. The mean fluorescence intensity calculated from Figure S7 (Supporting Information) exhibited a dose-dependent uptake behavior of nanoparticles by HeLa cells (Figure S8, Supporting Information).

3.5. Cytotoxicity and Distribution Pattern of Nanoparticles. For biomedical applications, the biocompatibility of particles is a critical issue. We examined the effect of HRP@HSN and HSN on cytotoxicity and cell proliferation in HeLa cells. After treatment with 0−100 μg/mL of particles for 2.5 h, HeLa cells were either processed with a cell viability assay using 2-(4-iodophenyl)-3-(4-nitrophenyl)-5-(2,4-disulfophenyl)-2H-tetrazolium (WST-1) for acute cytotoxicity determination (Figure S9a, Supporting Information) or further incubated in complete cell culture media for 24 h to evaluate cell proliferation (Figure S9b, Supporting Information). As shown in Figure S9 (Supporting Information), no obvious cytotoxicity was observed at 2.5 h of treatment of particles, nor was cell proliferation inhibited.

The cellular uptake of silica nanoparticles usually follows an endocytosis process. To determine whether HRP@F-HSN could escape the endosome, we treated the HeLa cells with uptaken HRP@F-HSN in the presence of an endosome marker (*N*-(3-triethylammoniumpropyl)-4-(4-diethylaminophenylhexatrienyl)pyridinium dibromide (FM4-64), red fluorescence). Figure 3b shows that some partial colocalization (yellow color) of HRP@F-HSN (green) and FM4-64 stained organelles (red). However, some particles may have escaped from endosome and aggregate in the cytosol (shows green dots). This is possibly due to the positively charged amine groups on the silica shell which would exert a "proton-sponge" effect.[40]

3.6. HRP@HSN as a Nonoreactor for Intracellular Biocatalysis Activating Prodrug. We evaluated the capability of HRP@HSN to intracellularly catalyze indole-3-acetic acid (IAA) to generate free radicals and to induce apoptosis in HeLa cells. After HRP@HSN was introduced to HeLa cells, the cells were washed twice with PBS to remove extracellular HRP@HSN. This is necessary to avoid extracellularly generated toxicity. Treated cells were then cultured with IAA and the cell viability by WST-1 test was determined 24 h later. We should comment here that the often-used MTT test cannot be used. Previously, it has been shown that mesoporous silica nanoparticles (MSNs), after being endocytosed, interfere with the MTT test in HeLa cells and astrocytes by accelerating the exocytosis of formazan crystals.[41] Thus, MTT reduction test gives an overestimation of the cytotoxicity of the silica nanoparticles compared to other tests such as LDH activity or the WST-1 test. Figure 4a shows the relative cell viabilities of particle-treated cells after exposure to 7.5 mM IAA for 24 h. In comparison with cells without nanoparticle treatment, native HRP and HSN did not cause cell death after incubation with 7.5 mM IAA. Notably, cell viability decreased with the increase of HRP@HSN dose but did not for that of the native HRP, implying that native HRP did not enter cells. This is consistent with literature report that native proteins were not ingested by cells;[42] in contrast, HRP@HSN is easily taken up by HeLa cells. We further analyzed the generated toxicity of HRP@HSN in combination with various concentrations of IAA. As shown in Figure 4b, with the increase of IAA doses, the IAA/HRP-induced cell death was enhanced. Compared with untreated cells (control), viability of HRP@HSN treated cells decreased approximately 10−25% at the IAA dose from 5 to 7.5 mM. By contrast, HSN-treated cells did not show any enhanced cytotoxicity. Thus, HRP@HSN could serve as a nanoreactor, converting IAA prodrug to free radicals intracellularly to kill cells. We should note here that, compared to other works on intracellular enzyme delivery,[43−46] we always have the enzyme protected inside the hollow silica nanospheres instead of

delivering to the cytosol. This would allow longer catalytic action before the final dissolution of the silica structure. The porous silica shell not only protects against proteolysis but also selectively allows transport of the small molecules of reactants and products.

4. CONCLUSIONS

We have reported a microemulsion-templating method for synthesizing hollow silica nanospheres. The method allows easy and mild conditions for encapsulating enzymes while the porous shell allows diffusion of small molecules, the substrates of the enzymes. This unique topology of HSN provides promising opportunities to serve as a nanoreactor in biomedical applications such as enzyme replacement therapy. In this work, we have demonstrated an application of this HSN-based nanoreactor on a prodrug-enzyme system to convert the nontoxic IAA into toxic free radicals by encapsulated HRP. We show both effective intracellular delivery of the HRP@HSN and subsequent decreased cellular viability.

In future developments, the large interior volume of HSN could, in principle, encapsulate multiple enzymes for cascade reactions or other drugs for synergistic effects. In contrast to other protein loading methods such as physical adsorption or direct conjugation on particle surface, our encapsulation strategy shielded protein from various denaturing or digestion agents. The external surface of HSN could be easily functionalized for cell targeting, elongation of blood circulation or attenuating antigenic and immunogenic responses. These multifunctionalities are favorable for further examination of enzyme therapy in future animal model studies.[47]

■ ASSOCIATED CONTENT

Ⓢ Supporting Information

TEM image of HSN stained with UA, enzyme leakage assay, HRP activity assay, confocal images of particle uptake, flow cytometry analysis of cellular uptake, cytotoxicity of particles and DLS sizes and zeta values of particles. This material is available free of charge via the Internet at http://pubs.acs.org.

■ AUTHOR INFORMATION

Corresponding Author

*C.-Y. Mou. E-mail: cymou@ntu.edu.tw.

Notes

The authors declare no competing financial interest.

■ ACKNOWLEDGMENTS

This research was funded by National Taiwan University and the National Science Council of Taiwan. We thank Ms. Chia-Ying Chien of Precious Instrument Center (National Taiwan University) for assistance with TEM experiments.

■ REFERENCES

(1) Tanner, P.; Egli, S.; Balasubramanian, V.; Onaca, O.; Palivan, C. G.; Meier, W. Can Polymeric Vesicles That Confine Enzymatic Reactions Act as Simplified Organelles? *FEBS Lett.* **2011**, *585*, 1699−1706.

(2) Palivan, C. G.; Fischer-Onaca, O.; Delcea, M.; Itel, F.; Meier, W. Protein-Polymer Nanoreactors for Medical Applications. *Chem. Soc. Rev.* **2012**, *41*, 2800−2823.

(3) Van Dongen, S. F. M.; Verdurmen, W. P. R.; Peters, R. J. R. W.; Nolte, R. J. M.; Brock, R.; van Hest, J. C. M. Cellular Integration of an Enzyme-Loaded Polymersome Nanoreactor. *Angew. Chem., Int. Ed.* **2010**, *49*, 7213−7216.

(4) Ben-Haim, N.; Broz, P.; Marsch, S.; Meier, W.; Hunziker, P. Cell-Specific Integration of Artificial Organelles Based on Functionalized Polymer Vesicles. *Nano Lett.* **2008**, *8*, 1368−1373.

(5) Tanner, P.; Onaca, O.; Balasubramanian, V.; Meier, W.; Palivan, C. G. Enzymatic Cascade Reactions inside Polymeric Nanocontainers: A Means to Combat Oxidative Stress. *Chem. −Eur. J.* **2011**, *17*, 4552−4560.

(6) De Vocht, C.; Ranquin, A.; Willaert, R.; Van Ginderachter, J. A.; Vanhaecke, T.; Rogiers, V.; Versees, W.; Van Gelder, P.; Steyaert, J. Assessment of Stability, Toxicity and Immunogenicity of New Polymeric Nanoreactors for Use in Enzyme Replacement Therapy of MNGIE. *J. Controlled Release* **2009**, *137*, 246−254.

(7) Reddy, M. K.; Labhasetwar, V. Nanoparticle-Mediated Delivery of Superoxide Dismutase to the Brain: An Effective Strategy to Reduce Ischemia-Reperfusion Injury. *FASEB J.* **2009**, *23*, 1384−1395.

(8) Batrakova, E. V.; Li, S.; Reynolds, A. D.; Mosley, R. L.; Bronich, T. K.; Kabanov, A. V.; Gendelman, H. E. A Macrophage-Nanozyme Delivery System for Parkinson's Disease. *Bioconjugate Chem.* **2007**, *18*, 1498−1506.

(9) Hasadsri, L.; Kreuter, J.; Hattori, H.; Iwasaki, T.; George, J. M. Functional Protein Delivery into Neurons Using Polymeric Nanoparticles. *J. Biol. Chem.* **2009**, *284*, 6972−6981.

(10) Popat, A.; Hartono, S. B.; Stahr, F.; Liu, J.; Qiao, S. Z.; Qing Max Lu, G. Q. Mesoporous Silica Nanoparticles for Bioadsorption, Enzyme Immobilisation, and Delivery Carriers. *Nanoscale* **2011**, *3*, 2801−2818.

(11) Yang, X.; Cai, Z.; Ye, Z.; Chen, S.; Yang, Y.; Wang, H.; Liu, Y.; Cao, A. In Situ Synthesis of Porous Silica Nanoparticles for Covalent Immobilization of Enzymes. *Nanoscale* **2012**, *4*, 414−416.

(12) Schlossbauer, A.; Schaffert, D.; Kecht, J.; Wagner, E.; Bein, T. Click Chemistry for High-Density Biofunctionalization of Mesoporous Silica. *J. Am. Chem. Soc.* **2008**, *130*, 12558−12559.

(13) Tang, L.; Cheng, J. Nonporous Silica Nanoparticles for Nanomedicine Application. *Nano Today* **2013**, *8*, 290−312.

(14) Lei, C.; Shin, Y.; Liu, J.; Ackerman, E. J. Entrapping Enzyme in a Functionalized Nanoporous Support. *J. Am. Chem. Soc.* **2002**, *124*, 11242−11243.

(15) Wang, Y. J.; Caruso, F. Mesoporous Silica Spheres as Supports for Enzyme Immobilization and Encapsulation. *Chem. Mater.* **2005**, *17*, 953−961.

(16) Sun, X.; Zhao, Y.; Lin, V. S.; Slowing, I. I.; Trewyn, B. G. Luciferase and Luciferin Co-Immobilized Mesoporous Silica Nanoparticle Materials for Intracellular Biocatalysis. *J. Am. Chem. Soc.* **2011**, *133*, 18554−18557.

(17) Slowing, I. I.; Trewyn, B. G.; Lin, V. S. Y. Mesoporous Silica Nanoparticles for Intracellular Delivery of Membrane-Impermeable Proteins. *J. Am. Chem. Soc.* **2007**, *129*, 8845−8849.

(18) Ashley, C. E.; Carnes, E. C.; Phillips, G. K.; Padilla, D.; Durfee, P. N.; Brown, P. A.; Hanna, T. N.; Liu, J. W.; Phillips, B.; Carter, M. B.; Carroll, N. J.; Jiang, X. M.; Dunphy, D. R.; Willman, C. L.; Petsev, D. N.; Evans, D. G.; Parikh, A. N.; Chackerian, B.; Wharton, W.; Peabody, D. S.; Brinker, C. J. The Targeted Delivery of Multicomponent Cargos to Cancer Cells by Nanoporous Particle-Supported Lipid Bilayers. *Nat. Mater.* **2011**, *10*, 476−476.

(19) Chen, J. F.; Ding, H. M.; Wang, J. X.; Shao, L. Preparation and Characterization of Porous Hollow Silica Nanoparticles for Drug Delivery Application. *Biomaterials* **2004**, *25*, 723−727.

(20) Li, Z. Z.; Wen, L. X.; Shao, L.; Chen, J. F. Fabrication of Porous Hollow Silica Nanoparticles and Their Applications in Drug Release Control. *J. Controlled Release* **2004**, *98*, 245−254.

(21) Zhou, J.; Wu, W.; Caruntu, D.; Yu, M. H.; Martin, A.; Chen, J. F.; O'Connor, C. J.; Zhou, W. L. Synthesis of Porous Magnetic Hollow Silica Nanospheres for Nanomedicine Application. *J. Phys. Chem. C* **2007**, *111*, 17473−17477.

(22) Huang, X.; Meng, X.; Tang, F.; Li, L.; Chen, D.; Liu, H.; Zhang, Y.; Ren, J. Mesoporous Magnetic Hollow Nanoparticles-Protein Carriers for Lysosome Escaping and Cytosolic Delivery. *Nanotechnology* **2008**, *19*, 445101.

(23) Lim, J. S.; Lee, K.; Choi, J. N.; Hwang, Y. K.; Yun, M. Y.; Kim, H. J.; Won, Y. S.; Kim, S. J.; Kwon, H.; Huh, S. Intracellular Protein Delivery by Hollow Mesoporous Silica Capsules with a Large Surface Hole. *Nanotechnology* **2012**, *23*, 085101.
(24) Cao, S. S.; Fang, L.; Zhao, Z. Y.; Ge, Y.; Piletsky, S.; Turner, A. P. F. Hierachically Structured Hollow Silica Spheres for High Efficiency Immobilization of Enzymes. *Adv. Funct. Mater.* **2013**, *23*, 2162−2167.
(25) Lou, X. W.; Archer, L. A.; Yang, Z. C. Hollow Micro-/Nanostructures: Synthesis and Applications. *Adv. Mater.* **2008**, *20*, 3987−4019.
(26) Wu, S. H.; Mou, C. Y.; Lin, H. P. Synthesis of Mesoporous Silica Nanoparticles. *Chem. Soc. Rev.* **2013**, *42*, 3862−3875.
(27) Chiu, Y. R.; Ho, W. J.; Chao, J. S.; Yuan, C. J. Enzyme-Encapsulated Silica Nanoparticle for Cancer Chemotherapy. *J. Nanopart. Res.* **2012**, *14*, 829−838.
(28) Folkes, L. K.; Wardman, P. Oxidative Activation of Indole-3-Acetic Acids to Cytotoxic Species − A Potential New Role for Plant Auxins in Cancer Therapy. *Biochem. Pharmacol.* **2001**, *61*, 129−136.
(29) De Melo, M. P.; de Lima, T. M.; Pithon-Curi, T. C.; Curi, R. The Mechanism of Indole Acetic Acid Cytotoxicity. *Toxicol. Lett.* **2004**, *148*, 103−111.
(30) Lin, Y. S.; Wu, S. H.; Tseng, C. T.; Hung, Y.; Chang, C.; Mou, C. Y. Synthesis of Hollow Silica Nanospheres with a Microemulsion as the Template. *Chem. Commun.* **2009**, 3542−3544.
(31) Ow, H.; Larson, D. R.; Srivastava, M.; Baird, B. A.; Webb, W. W.; Wiesner, U. Bright and Stable Core-Shell Fluorescent Silica Nanoparticles. *Nano Lett.* **2005**, *5*, 113−117.
(32) Muddana, H. S.; Morgan, T. T.; Adair, J. H.; Butler, P. J. Photophysics of Cy3-Encapsulated Calcium Phosphate Nanoparticles. *Nano Lett.* **2009**, *9*, 1559−1566.
(33) Dziubla, T. D.; Shuvaev, V. V.; Hong, N. K.; Hawkins, B. J.; Madesh, M.; Takano, H.; Simone, E.; Nakada, M. T.; Fisher, A.; Albelda, S. M.; Muzykantov, V. R. Endothelial Targeting of Semi-Permeable Polymer Nanocarriers for Enzyme Therapies. *Biomaterials* **2008**, *29*, 215−227.
(34) Fornera, S.; Walde, P. Spectrophotometric Quantification of Horseradish Peroxidase with O-Phenylenediamine. *Anal. Biochem.* **2010**, *407*, 293−295.
(35) Karimi, B.; Emadi, S.; Safari, A. A.; Kermanian, M. Immobilization, Stability and Enzymatic Activity of Albumin and Trypsin Adsorbed onto Nanostructured Mesoporous Sba-15 with Compatible Pore Sizes. *RSC Adv.* **2014**, *4*, 4387−4394.
(36) Lin, W. I.; Lin, C. Y.; Lin, Y. S.; Wu, S. H.; Huang, Y. R.; Hung, Y.; Chang, C.; Mou, C. Y. High Payload Gd(Iii) Encapsulated in Hollow Silica Nanospheres for High Resolution Magnetic Resonance Imaging. *J. Mater. Chem. B* **2013**, *1*, 639−645.
(37) Zhu, Y. F.; Shi, J. L.; Shen, W. H.; Dong, X. P.; Feng, J. W.; Ruan, M. L.; Li, Y. S. Stimuli-Responsive Controlled Drug Release from a Hollow Mesoporous Silica Sphere/Polyelectrolyte Multilayer Core-Shell Structure. *Angew. Chem., Int. Ed.* **2005**, *44*, 5083−5087.
(38) Meng, H.; Liong, M.; Xia, T.; Li, Z.; Ji, Z.; Zink, J. I.; Nel, A. E. Engineered Design of Mesoporous Silica Nanoparticles to Deliver Doxorubicin and P-Glycoprotein Sirna to Overcome Drug Resistance in a Cancer Cell Line. *ACS Nano* **2010**, *4*, 4539−4550.
(39) Lundqvist, M.; Stigler, J.; Elia, G.; Lynch, I.; Cedervall, T.; Dawson, K. A. Nanoparticle Size and Surface Properties Determine the Protein Corona with Possible Implications for Biological Impacts. *Proc. Natl. Acad. Sci. U. S. A.* **2008**, *105*, 14265−14270.
(40) Akinc, A.; Thomas, M.; Klibanov, A. M.; Langer, R. Exploring Polyethylenimine-Mediated DNA Transfection and the Proton Sponge Hypothesis. *J. Gene Med.* **2005**, *7*, 657−663.
(41) Fisichella, M.; Dabboue, H.; Bhattacharyya, S.; Saboungi, M. L.; Salvetat, J. P.; Hevor, T.; Guerin, M. Mesoporous Silica Nanoparticles Enhance Mtt Formazan Exocytosis in Hela Cells and Astrocytes. *Toxicol. In Vitro* **2009**, *23*, 697−703.
(42) Yan, M.; Du, J. J.; Gu, Z.; Liang, M.; Hu, Y. F.; Zhang, W. J.; Priceman, S.; Wu, L. L.; Zhou, Z. H.; Liu, Z.; Segura, T.; Tang, Y.; Lu, Y. F. A Novel Intracellular Protein Delivery Platform Based on Single-Protein Nanocapsules. *Nat. Nanotechnol.* **2010**, *5*, 48−53.
(43) Tamura, A.; Ikeda, G.; Seo, J. H.; Tsuchiya, K.; Yajima, H.; Sasaki, Y.; Akiyoshi, K.; Yui, N. Molecular Logistics Using Cytocleavable Polyrotaxanes for the Reactivation of Enzymes Delivered in Living Cells. *Sci. Rep.* **2013**, *3*, 2252.
(44) Wu, X. J.; Wu, S. Q.; Yang, L.; Han, J. H.; Han, S. F. Cytosolic Delivery of Proteins Mediated by Aldehyde-Displaying Silica Nanoparticles with Ph-Responsive Characteristics. *J. Mater. Chem.* **2012**, *22*, 17121−17127.
(45) Tang, R.; Kim, C. S.; Solfiell, D. J.; Rana, S.; Mout, R.; Velazquez-Delgado, E. M.; Chompoosor, A.; Jeong, Y.; Yan, B.; Zhu, Z. J.; Kim, C.; Hardy, J. A.; Rotello, V. M. Direct Delivery of Functional Proteins and Enzymes to the Cytosol Using Nanoparticle-Stabilized Nanocapsules. *ACS Nano* **2013**, *7*, 6667−6673.
(46) Ghosh, P.; Yang, X. C.; Arvizo, R.; Zhu, Z. J.; Agasti, S. S.; Mo, Z. H.; Rotello, V. M. Intracellular Delivery of a Membrane-Impermeable Enzyme in Active Form Using Functionalized Gold Nanoparticles. *J. Am. Chem. Soc.* **2010**, *132*, 2642−2645.
(47) Torchilin, V. Intracellular Delivery of Protein and Peptide Therapeutics. *Drug Discovery Today: Technol.* **2008**, *5*, e95−e103.